J. Phys. Chem. **1994,** *98,* 10173–10179

^{129}Xe NMR Study of TiO_2 (Anatase)-Supported V_2O_5 Catalysts

Jürgen Kritzenberger, Holly C. Gaede, Jay S. Shore, and Alex Pines*

Materials Sciences Division, Lawrence Berkeley Laboratory and Department of Chemistry,
University of California, Berkeley, California 94720

Alexis T. Bell

Chemical Sciences Division, Lawrence Berkeley Laboratory and Department of Chemical Engineering,
University of California, Berkeley, California 94720

Received: January 10, 1994; In Final Form: May 31, 1994®

TiO_2 (anatase), V_2O_5, and V_2O_5/TiO_2 (anatase) catalysts with 1.3%, 3.0%, and 9.8% weight loadings of V_2O_5 have been studied using temperature-dependent xenon-129 NMR spectroscopy. The intrinsic chemical shift values due to the interaction of xenon with the surface are 109 ± 3 ppm for TiO_2 (anatase) and 93 ± 5 ppm for V_2O_5. The V_2O_5/TiO_2 catalysts provide strong adsorption sites for xenon which cause an initial decrease of the chemical shift values at low xenon loadings. Additionally, the spectra of pure V_2O_5 reveal two distinct environments for the xenon atoms, consistent with the hysteresis of the isotherm and the existence of pores. Two-dimensional exchange spectroscopy was used to measure the rates and activation energy of xenon moving between these two environments.

Introduction

Supported V_2O_5 is used as a catalyst for the selective oxidation of hydrocarbons[1-3] and for the selective reduction of nitrogen oxides.[4] A high catalytic activity and selectivity are achieved when vanadia is present as a highly dispersed, amorphous species.[3,5,6] The exact structure of the amorphous vanadia dispersed on the support is the focus of several recent reports.[7-11] *In situ* laser Raman spectroscopy[12] indicates that V_2O_5/TiO_2 (anatase) catalysts contain monomeric vanadyl and polymeric vanadate species, as well as crystallites of V_2O_5. At low vanadia loadings the monomeric species predominate, and with increasing loading, polymeric vanadates are formed. Crystallites of V_2O_5 are formed if the vanadia loading is larger than the monolayer capacity of the support.

In this paper we apply ^{129}Xe NMR to study V_2O_5/TiO_2 (anatase), illustrating the potential of ^{129}Xe NMR to study metal oxide-supported catalysts. Following the pioneering work of Fraissard and co-workers,[13-19] ^{129}Xe NMR has become a useful technique for the investigation of porous solids such as zeolites.[20-27] The large polarizability of the electron cloud of xenon accounts for its adsorption properties and the large NMR chemical shift range of atomic xenon of ~350 ppm. These properties together with its chemical inertness make xenon an excellent probe of local environments, including the structural features of molecular sieves[13-18] and the effects of hydration.[19] Ryoo et al.[28] have used this method to examine the physical mixing of composite catalysts. Bansal and Dybowski[29] have measured the diffusivity of water in Ni–NaY by observing the change of the xenon chemical shift with time. ^{129}Xe NMR has also been used to study the distribution of different organic molecules in zeolite NaY.[30-32] Several reviews[33-36] give an overview of the use of ^{129}Xe NMR as a probe for the study of porous solids.

In contrast to the extensive work in the field of zeolites, there are only a few ^{129}Xe NMR studies of amorphous materials. Cheung[37] has reported the effects of pore size distribution of silica, alumina, and silica–alumina on the xenon chemical shift. Conner et al.[38] have used xenon as a probe of the pore structure created by compression of nonporous silica.

The use of xenon as a probe of metal cluster formation in zeolites is facilitated by the presence of strong adsorption sites for the xenon atoms on the metal particles. The nonlinear behavior of the chemical shift at low xenon loadings is a useful tool for the study of the exchange of cations in zeolites and metal cluster formation and growth on zeolites.[16,21,23,24,39,40] Boudart et al.[41-43] have applied this method to study chemisorption of H_2 and O_2 on platinum particles supported on alumina. In this work, ^{129}Xe NMR was used to investigate structural features of V_2O_5, TiO_2 (anatase), and V_2O_5/TiO_2 (anatase) catalysts, extending the application of this technique to study metal oxides on supports, enabling the selective investigation of the dispersed metal oxide.

Experimental Section

Apparatus. The experimental apparatus consists of a xenon reservoir connected by glass tubing to a sample ampule located in a 4.2 T superconducting magnet.[44] A connection to a vacuum rack allows the sample region to be evacuated. The pressure in the sample region is measured by a thermocouple pressure gauge.

The NMR probe consists of a Macor ceramic coil support, glass dewar, dewared stainless steel transfer line for the nitrogen cooling gas, and a glass transfer line for the xenon. The sample region contains a radio-frequency-shielded thermocouple for monitoring and controlling the temperature during the experiments. We used a temperature range between 133 and 300 K, which could be controlled within ±1 K.

The sample was slowly cooled and brought to thermal equilibrium at the desired temperature. After adding a known amount of xenon, we typically waited 2 min for equilibrium before acquiring data. For all NMR experiments we used 80% enriched ^{129}Xe (EG+G Mound Miamisburg, OH). After we acquired an NMR spectrum, the sample was allowed to warm and the xenon was recovered by condensing it with liquid nitrogen.

The spectra were acquired by Fourier transformation of the signal obtained after a 90° radio-frequency pulse. The chemical

---

® Abstract published in *Advance ACS Abstracts,* September 1, 1994.

0022-3654/94/2098-10173$04.50/0

shifts are referenced to an external standard of dilute gas-phase xenon.[45] The number of scans necessary to achieve a good signal-to-noise ratio was strongly dependent on the surface area of the sample, temperature, and xenon pressure. For example, 64 scans were required for the 1.3% V_2O_5/TiO_2 sample at 153 K and 32 768 scans were required for the pure V_2O_5 sample at 300 K. Typical NMR pulse recycle times were between 0.1 and 1 s.

For the 2D exchange experiments,[46] V_2O_5 was flame-sealed in a Pyrex ampule (10 mm o.d.) with approximately 2 atm of 80% enriched ^{129}Xe. The ^{129}Xe NMR spectra were acquired at 11.7 T (138.3 MHz) with a Chemagnetics CMX-500 spectrometer and a 90° rf pulse of 5 μs. A typical recycle time was 300 ms. We used a standard pulse sequence and the method of States *et al.*[47] to obtain pure adsorption spectra. Typically, 128 and 256 points were acquired in t_1 and t_2, respectively, with 256 scans per t_1 value. During data processing, the t_1 dimension was zero-filled to 256 points and 100 Hz Gaussian line broadening was applied in both dimensions.

Catalyst Preparation and Pretreatment. The preparation of the V_2O_5/TiO_2 samples is described in detail elsewhere.[12] The weight percent loading of V_2O_5 on the surface of TiO_2 (anatase) is shown as *X*% V_2O_5/TiO_2 (X = 1.3, 3.0, or 9.8). We used commercially available TiO_2 (anatase) (Aldrich Gold Label, 99.9%) and V_2O_5 (Aldrich, 98%+).

Contamination by water is the main obstacle in the preparation of clean metal oxide surfaces.[48,49] The samples were heated to 400 °C under vacuum ($<10^{-4}$ Torr) to remove surface bound water and then heated in an O_2 atmosphere (300 Torr) at the same temperature for 1 h to produce a fully oxidized surface. The samples were then loaded into the NMR probe and immediately evacuated to 10^{-5} Torr. When loading the samples into the probe, the samples were exposed to atmosphere for approximately 1 min. To remove any water adsorbed during this time, the samples were heated to 200 °C under vacuum ($<10^{-5}$ Torr) for 2 h. It was possible to monitor the desorption of water with a pressure gauge. After a short time of heating an increase in pressure was observed, followed by a slow decrease to the original value ($<10^{-5}$ Torr). The sample was then heated (200 °C) for 1 h under oxygen (300 Torr), the probe was transferred into the magnet, and the sample was evacuated to a pressure below 10^{-5} Torr for 12 h at room temperature.

Isotherms. Nitrogen and xenon isotherms were measured to determine the surface areas and adsorption energies of xenon on the metal oxide samples. The data show a BET[50] like behavior (Figure 1). The equation for a BET isotherm is

$$V = \frac{V_{\mathrm{mon}} c x}{(1 - x)[1 + x(c - 1)]} \qquad (1)$$

where V is the volume of adsorbed gas at STP, $x = p/p_0$ is the reduced pressure, and V_{mon} is the volume that would be occupied at STP by the amount of gas needed to form a monolayer on 1 g of sample. The quantity c is related to the adsorption energy, ΔH_{ads}, by the equation

$$\ln c = (\Delta H_{\mathrm{ads}} - \Delta H_{\mathrm{l}})/RT \qquad (2)$$

where ΔH_{l} is the heat of liquefaction of the adsorbate (3.57 kcal/mol).[51] The nitrogen and xenon isotherms were measured on a glass vacuum rack using a silicone oil diffusion pump capable of pressures below 10^{-5} Torr. For the xenon isotherms we used cold-temperature baths of the following organic solvents cooled with liquid nitrogen: *n*-pentane (143 K), methanol (172 K), and ethyl acetate (190 K). For accuracy, the dead-volume measurements using helium gas were made at each temperature for which an isotherm was measured.

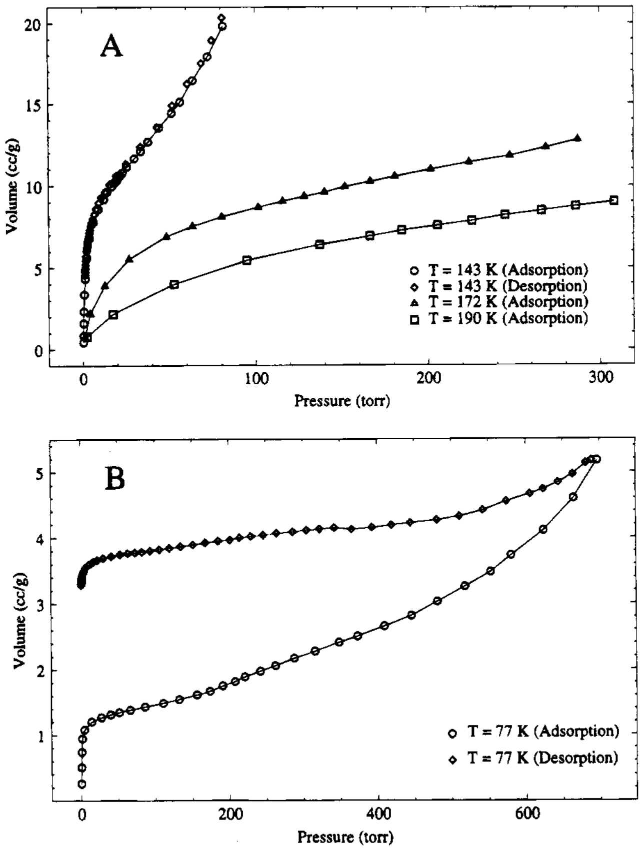

Figure 1. (A) BET isotherms of xenon on 3.0% V_2O_5/TiO_2 (anatase) at 143 K (adsorption and desorption), 172 K (adsorption), and 190 K (adsorption). (B) BET adsorption and desorption isotherm of nitrogen on V_2O_5. In both figures, lines connect the points to guide the eye.

TABLE 1: Isotherm Data for Nitrogen and Xenon Adsorbed onto TiO_2 (Anatase), 1.3% V_2O_5/TiO_2 (Anatase), 3.0% V_2O_5/TiO_2 (Anatase), 9.8% V_2O_5/TiO_2 (Anatase), and V_2O_5

sample	gas	temp (K)	ΔH_{ads} (kcal/mol)	BET surface area (m^2/g)
TiO_2	N_2	77	2.1	9
	Xe	143	4.6	7
	Xe	172	4.5	8
	Xe	190	4.2	18
1.3% V_2O_5/TiO_2	N_2	77	2.0	86
	Xe	143	4.8	81
	Xe	172	4.9	73
	Xe	190	4.9	79
3.0% V_2O_5/TiO_2	N_2	77	2.1	69
	Xe	143	4.9	59
	Xe	172	4.8	63
	Xe	190	4.7	70
9.8% V_2O_5/TiO_2	N_2	77	2.1	27
	Xe	143	4.9	24
	Xe	172	4.9	24
	Xe	190	4.7	28
V_2O_5	N_2	77	2.1	6
	Xe	143	5.0	5
	Xe	172	4.4	7
	Xe	190	4.3	11

In Figure 1A the xenon isotherms of the 3.0% V_2O_5/TiO_2 sample are presented. The isotherms at 143, 172, and 190 K show characteristic BET behavior for all samples used in this study. The parameters used for the xenon and nitrogen isotherms are listed in Table 1. In accord with the BET theory, the heat of adsorption (ΔH_{ads}) was determined from the linear

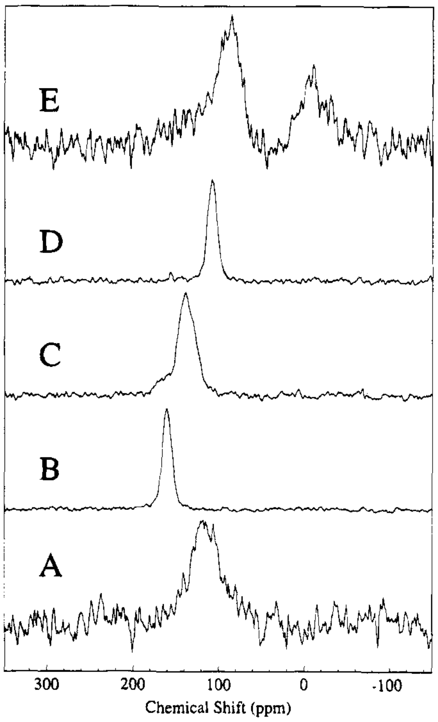

Figure 2. Representative ^{129}Xe NMR spectra at 4.2 T (49.45 MHz) of xenon adsorbed on (A) TiO_2 ($T = 172$ K, $\Theta = 0.59$), (B) 1.3% V_2O_5/TiO_2 ($T = 172$ K, $\Theta = 0.62$), (C) 3.0% V_2O_5/TiO_2 ($T = 173$ K, $\Theta = 0.63$), (D) 9.8% V_2O_5/TiO_2 ($T = 173$ K, $\Theta = 0.58$), and (E) V_2O_5 ($T = 213$ K, $\Theta = 0.34$); the poor S/N of spectra A and E is due to the low surface area of the TiO_2 anatase and the V_2O_5 sample (see Table 1).

region of the isotherm (reduced pressure $0.05 \le x \le 0.3$). Note that in this pressure range the isotherms are insensitive to the presence of a small number of strong adsorption sites. The absence of hysteresis for the xenon isotherm taken at 143 K indicates that the sample does not contain pores. In contrast, for V_2O_5 the nitrogen adsorption and desorption isotherms display extreme hysteresis, indicating the presence of dead-ended and ink-bottle pores with a wide range of pore sizes.[52,53] To analyze the chemical shift data for xenon on the V_2O_5/TiO_2 samples, we determined V_{mon} from the N_2 isotherms. Knowing p_0 from saturated vapor pressure measurements,[54,55] eq 1 was used to calculate the coverage Θ, which is equal to V/V_{mon}. Values for c were obtained from fits of the isotherms to eq 1 for each of the temperatures used in the NMR experiments. The heats of adsorption were determined using eq 2 and are presented in Table 1.

Results and Discussion

Representative spectra of ^{129}Xe adsorbed on TiO_2 (spectrum A), on V_2O_5/TiO_2 with different V_2O_5 weight loadings (spectra B–D), and on V_2O_5 (spectrum E) are presented in Figure 2. For the pure TiO_2 (anatase) as well as for the V_2O_5/TiO_2 catalysts there is a single xenon peak. In contrast, two distinct resonances for xenon on V_2O_5 are observed. The poor signal-to-noise ratios of spectra A and E are due to the low surface areas of the TiO_2 (anatase) and the V_2O_5 samples (see Table 1). At the temperatures at which the spectra were acquired, xenon is mobile and on the NMR time scale ($\sim 10^{-3}$ s) samples both the surface and gas phase. Because of this motion, ^{129}Xe NMR spectra do not usually contain anisotropic line shapes from adsorption interactions; however, anisotropic line shapes have been observed for xenon in cavities.[56,57] The spectra displayed in Figure 2 were obtained using xenon coverages, Θ, between 0.34 and 0.63.

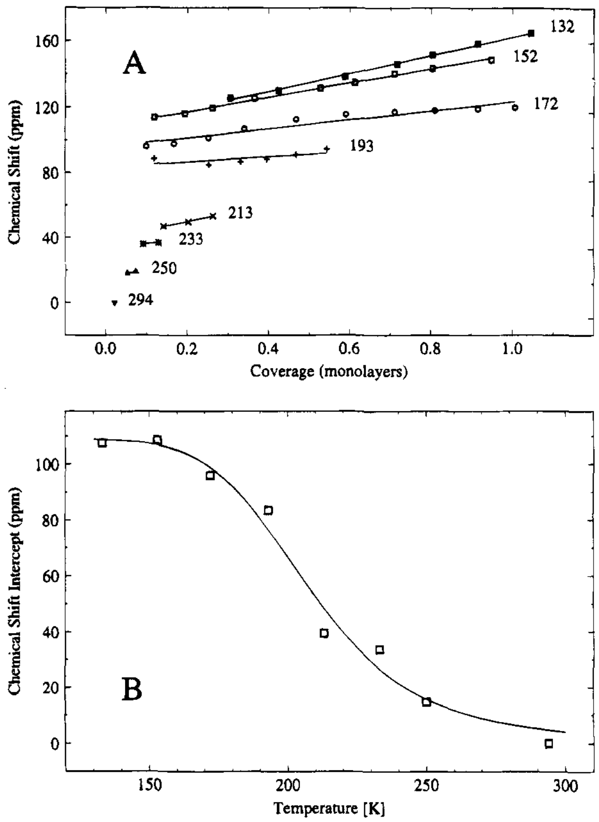

Figure 3. (A) ^{129}Xe chemical shift (ppm) of xenon adsorbed on TiO_2 (anatase) as a function of the temperature (K) and coverage (in monolayers). Lines represent linear least-squares fits to the data at each temperature. (B) ^{129}Xe chemical shift intercepts (ppm) of xenon adsorbed on TiO_2 (anatase) versus temperature.

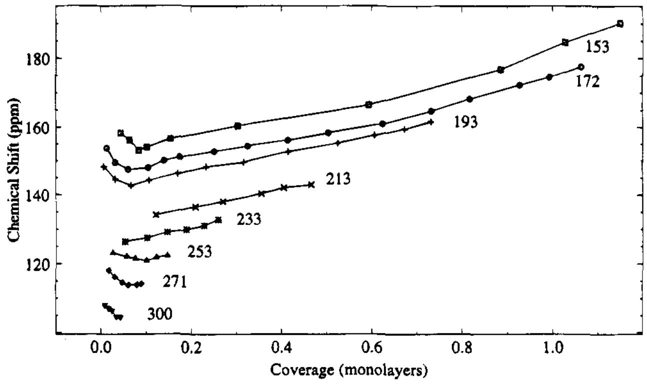

Figure 4. ^{129}Xe chemical shift (ppm) of xenon adsorbed on 1.3% V_2O_5/TiO_2 (anatase) as a function of temperature (K) and coverage (in monolayers). Lines connect the points at each temperature to guide the eye.

The chemical shifts of xenon adsorbed on the surfaces of TiO_2 (anatase), V_2O_5/TiO_2, and V_2O_5 as a function of temperature and coverage are displayed in Figures 3–7. The chemical shift of ^{129}Xe adsorbed on the surface of pure TiO_2 (anatase) as well as pure V_2O_5 shows a linear dependence on the xenon coverage. In contrast, the shifts of xenon adsorbed on V_2O_5/TiO_2 catalysts initially decrease with increasing coverage and then with greater coverage increase due to xenon–xenon interactions near the surface.[44]

Xenon Adsorbed on TiO_2 (Anatase). The shift of xenon adsorbed on pure TiO_2 (anatase) results from rapid exchange of the xenon atoms between the gas phase and the surface-

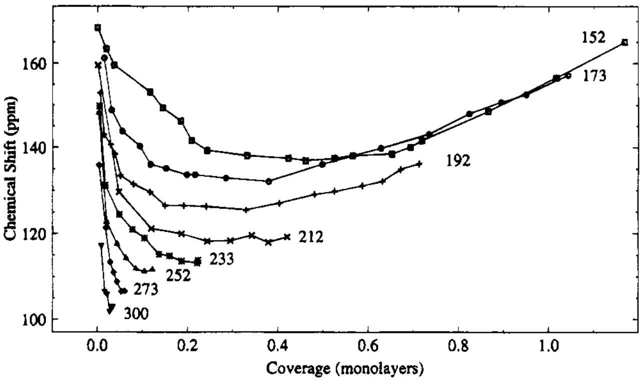

Figure 5. ^{129}Xe chemical shift (ppm) of xenon adsorbed on 3.0% V_2O_5/TiO_2 (anatase) as a function of temperature (K) and coverage (in monolayers). Lines connect the points at each temperature to guide the eye.

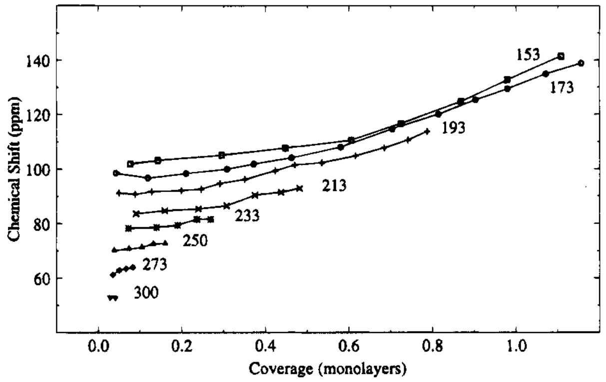

Figure 6. ^{129}Xe chemical shift (ppm) of xenon adsorbed on 9.8% V_2O_5/TiO_2 (anatase) as a function of temperature (K) and coverage (in monolayers). Lines connect the points at each temperature to guide the eye.

adsorbed phase. Hence, the total chemical shift is equal to the shift due to interactions at the surface (δ_s) plus that of the gas phase (δ_g), weighted by the relative probabilities of the xenon atom being on the surface ($P_s(T)$) and in the gas phase ($P_g(T)$).

$$\delta(T,\Theta) = \delta_g(T,\Theta)\,P_g(T) + \delta_s(T,\Theta)\,P_s(T) \qquad (3)$$

The shift of xenon at low pressure is used as an external standard and defined as 0 ppm. The temperature and pressure dependences of the chemical shift of xenon gas have been found to be small[58] and can be neglected in this study. Hence, the measured shift is simply the shift due to interactions at the surface (δ_s) multiplied by the probability of being at the surface ($P_s(T)$).

Raftery *et al.*[44] have shown that the shift due to interactions at the surface can be written in a virial-type expansion

$$\delta_s(T,\Theta) = \sigma_0 + \sigma_1\Theta P_s(T) + \sigma_2(\Theta P_s(T))^2 + \sigma_3(\Theta P_s(T))^3 + ... \qquad (4)$$

where σ are the virial coefficients of the nuclear shielding and, for our work, are considered temperature independent.[58] The first term in the expansion (σ_0) is due to interactions between xenon and the surface. The second term results from xenon–xenon interactions at or near the surface. The linear dependence of the chemical shift on coverage (Figure 3A) indicates that higher-order terms can be neglected and that only binary collisions between xenon atoms near the surface appear to be important at the xenon coverages studied. The slope of the shift as a function of coverage results from the binary xenon–xenon collisions at or near the surface.[44]

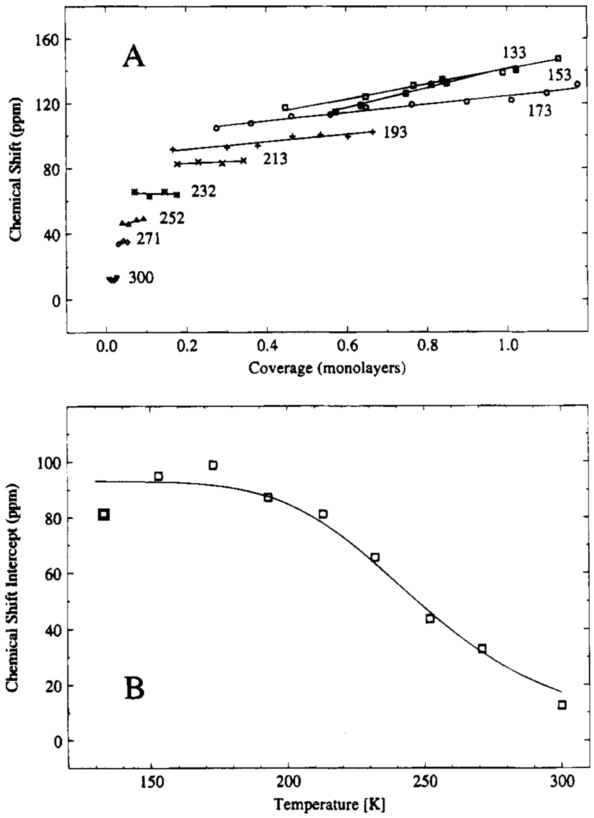

Figure 7. (A) ^{129}Xe chemical shift (ppm) of xenon adsorbed on V_2O_5 as a function of the temperature (K) and coverage (in monolayers). Included are only shift values of the resonance attributed to xenon adsorbed on the surface of V_2O_5 in rapid exchange with gas phase xenon (see text for details). Lines represent linear least-squares fits to the data at each temperature. (B) ^{129}Xe chemical shift intercepts (ppm) of xenon adsorbed on V_2O_5 versus temperature.

The chemical shift of the adsorbed xenon resonances extrapolated to zero coverage ($\delta(T,\Theta=0)$) is

$$\delta(T,\Theta=0) = \sigma_0 P_s(T) \qquad (5)$$

dependent on only the xenon–surface interactions and probability of the xenon being on the surface. The probability of finding a xenon atom at the surface can be written as[44]

$$P_s(T) = \tau_s/(\tau_s + \tau_v) \qquad (6)$$

where τ_s is the sticking time and τ_v is the mean time between sticking collisions of xenon with the surface. The average sticking time is given by

$$\tau_s = \tau_0 e^{\Delta H_{ads}/kT} \qquad (7)$$

where τ_0 is the preexponential factor and ΔH_{ads} is the energy of adsorption. Combining eqs 5–7 yields

$$\delta(T,\Theta=0) = \sigma_0 \frac{e^{\Delta H_{ads}/kT}}{\tau_v/\tau_0 + e^{\Delta H_{ads}/kT}} \qquad (8)$$

With the heat of adsorption given in Table 1, we fit the chemical shift extrapolated to zero coverage, $\delta(T,\Theta=0)$, as a function of temperature, to eq 8. The fit and data are presented in Figure 3B. The contribution to the chemical shift due to xenon–surface interactions (σ_0) is found to be 109 ppm for TiO_2 (anatase), compared to 86 ppm measured for xenon in NaY zeolite at 144 K[59] and 120–150 ppm for amorphous silica, silica–alumina, and alumina at 144 K.[37] For the ratio τ_v/τ_0 we

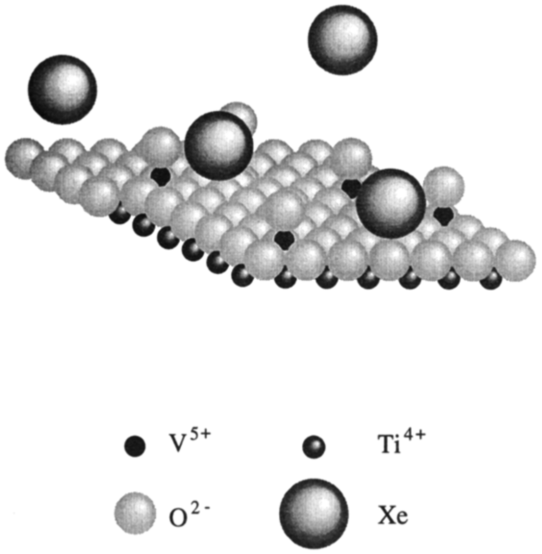

Figure 8. Schematic drawing of xenon exposed to a TiO_2 surface loaded with monomeric vanadia units. We used the radii 0.59 Å for V^{5+},[61] 0.68 Å for Ti^{4+},[61] 1.32 Å for O^{2-},[61] and 2.2 Å for Xe[23,34] to represent the different elements.

find a value of 4×10^4, which is comparable to that determined for xenon on a polymer surface (3×10^4).[44]

Xenon Adsorbed on V_2O_5/TiO_2 Catalysts. The chemical shifts as a function of coverages for the loaded V_2O_5/TiO_2 samples are shown in Figures 4–6. An initial decrease in the chemical shift with coverage is attributed to interactions of xenon atoms with a limited number of strong adsorption sites.[16,21,23,24,39,40] The most attractive adsorption sites are occupied first and cause an initial high shift value. With increasing coverage only less attractive sites are available for xenon, which causes a decrease in the average chemical shift. This proceeds until the increasing xenon–xenon interactions begin to dominate the xenon–surface interactions and cause an increase in the chemical shift at higher coverages.

On a pure TiO_2 surface the chemical shift of xenon shows a linear dependence on the coverage. A dramatic change in the chemical shift behavior of xenon occurs if a small amount of V_2O_5 is introduced to the surface (Figure 4). Compared to pure TiO_2, the chemical shift values of xenon extrapolated to zero pressure are larger by 50 ppm at 153 K and by 100 ppm at room temperature. In addition, the chemical shift of xenon decreases at low xenon coverages, which suggests the presence of strong adsorption sites. According to Went *et al.*[12] the surface of the 1.3% V_2O_5/TiO_2 catalyst is composed of 80% monomeric vanadium oxide units and 20% polymeric units. The vanadium atoms of the surface vanadium oxide are accessible to the xenon atoms and provide strong adsorption sites for xenon (Figure 8).

With increasing V_2O_5 loading, the space between the vanadium oxide units decreases, and correspondingly the capacity for xenon atoms in contact with strong adsorption sites decreases (Figure 8). Additionally, the increased loading causes a decrease of the fraction of monomeric species and an increase of the fraction of polymeric species.[12] However, the space between monomeric units is drastically reduced; hence, the average time xenon spends close to vanadium atoms is increased. Increased loading of vanadia is expected to have two effects on the chemical shift of xenon: there will be fewer strong sites available for the xenon; however, the chemical shift due to these sites is greater because the xenon is spending more time on or near these sites. A comparison of the chemical shift data of the 3.0% V_2O_5/TiO_2 sample (Figure 5) to that of the 1.3% V_2O_5/TiO_2 sample (Figure 4) seems to confirm this hypothesis. The xenon chemical shift values on the 3.0% V_2O_5/TiO_2 sample are larger at very low coverages and smaller at higher coverages than for xenon on the 1.3% V_2O_5/TiO_2 sample (Figure 4). This initial larger chemical shift implies that the xenon interacts more strongly with the 3.0% V_2O_5/TiO_2 surface than the 1.3% V_2O_5/TiO_2 surface. The smaller shift at higher coverages may indicate, however, that there are fewer total adsorption sites available for xenon on the 3.0% V_2O_5/TiO_2 sample.

A further increase of the vanadium content to 9.8 wt % V_2O_5 produces a monolayer of vanadium oxide on TiO_2 and V_2O_5 crystallites are formed.[12] A complete layer of vanadium oxide on the surface decreases the accessibility of xenon to strong adsorption sites (vanadium atoms), which is reflected in the shift data (Figure 6). There is no decrease of the xenon chemical shift for low xenon loadings, and the chemical shift is almost linearly dependent on coverage; both observations are expected for surfaces without a limited number of strong adsorption sites.

Unfortunately, it is not currently possible to develop a quantitative interpretation of our xenon shift data due to the complex nature of the xenon–surface interactions. The chemical shift of a xenon atom on the surface of V_2O_5/TiO_2 is influenced not only by the total number of vanadium atoms present but also by the distance between the vanadia groups and the actual structure of the surface.

Xenon Adsorbed on V_2O_5. The ^{129}Xe NMR spectrum of xenon adsorbed on V_2O_5 has two well-resolved peaks (Figure 2E), due to two distinct environments for xenon. The relative intensity of the peaks change with temperature. At 173 K, only the peak at higher frequency is detected. With increasing temperature the relative intensity of this peak decreases, which is characteristic of an adsorbed species. Also, this resonance shows a pressure and temperature dependence similar to that of xenon adsorbed on TiO_2. Hence, it is attributed to xenon adsorbed on the surface of V_2O_5 in rapid exchange with gas phase xenon. The resonance at ~0 ppm appears to be from xenon in a gas like environment, as evidenced by the chemical shift. The peak assignments are further discussed below.

For xenon adsorbed on V_2O_5 in rapid exchange with gas phase xenon (the peak at higher frequency), it is possible to apply the same formalism used to interpret the xenon chemical shift of xenon adsorbed on TiO_2 (Figure 3B). As in the case of TiO_2, the chemical shift shows a linear dependence on coverage (Figure 7A), which indicates that only binary collisions between xenon atoms are important at the xenon coverages studied. Figure 7B shows the temperature dependence of the chemical shift intercepts, $\delta(T,\Theta=0)$, for this resonance. The fit to eq 8 yields a chemical shift due to xenon–surface interactions (σ_0) for V_2O_5 of 93 ppm. For the ratio τ_v/τ_0 we obtain a value of 9×10^3.

To further investigate the relationship of the two peaks observed in the ^{129}Xe NMR spectrum for V_2O_5, we used two-dimensional (2D) exchange spectroscopy,[46,47] which is a useful tool for studying dynamics.[60] In Figures 9 and 10 the ^{129}Xe two-dimensional exchange NMR spectra of xenon adsorbed on V_2O_5 using the mixing times indicated are presented. The diagonal peaks correspond to ^{129}Xe resonances from xenon atoms in two different environments. The cross-peaks result from motion of xenon between the two distinct environments during the mixing time of the 2D experiment and have intensities that are proportional to the number of xenon that exchanged. By fitting the intensity of the cross-peak divided by the intensity of the adsorbed peak as a function of mixing time to an exponential function, we obtained the following rate constants

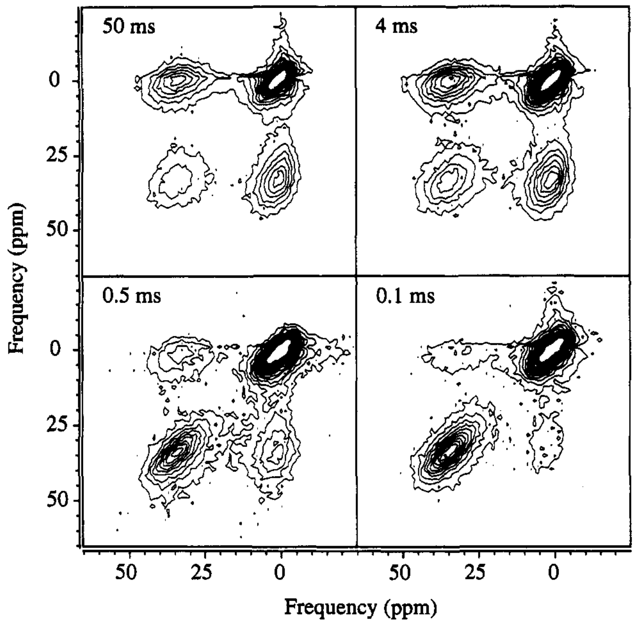

Figure 9. ^{129}Xe 2D exchange NMR spectra, at 11.7 T (138 MHz), of xenon adsorbed on V_2O_5 at 290 K and a xenon pressure of approximately 2 atm. The spectra were acquired using mixing times of 50, 4, 0.5, and 0.1 ms and a recycle delay of 300 or 500 ms. The contour lines represent 1% to 20% of the maximum intensity.

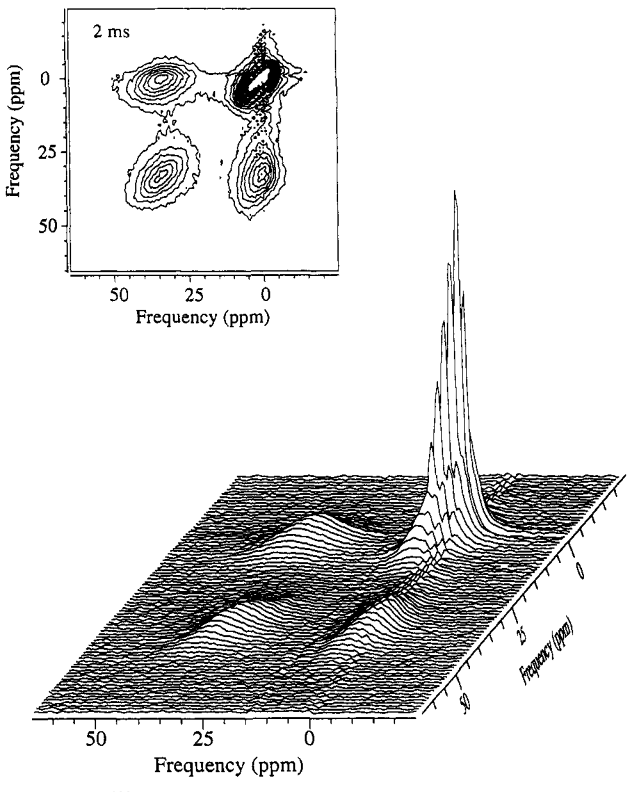

Figure 10. ^{129}Xe 2D exchange NMR spectrum, at 11.7 T (138 MHz), of xenon adsorbed on V_2O_5 at 290 K and a xenon pressure of approximately 2 atm. The spectrum was acquired using a mixing time of 2 ms and a recycle delay of 300 ms. The contour lines represent 1−20% of the maximum intensity.

($1/\tau$) for the exchange of xenon between the two environments: 0.78, 0.91, and 1.45 ms^{-1} for temperatures of 210, 250, and 290 K, respectively. These rate constants are consistent with an activation energy of 0.24 ± 0.09 kcal/mol. A distance between the two xenon environments of 5×10^{-5} m can be estimated from the rate constants assuming nonactivated diffusion. The diameter of the particles of the V_2O_5 are between 1.5×10^{-4} and 3.0×10^{-4} m. Also, using these rates, the width of the peaks due to exchange broadening can be approximated by $(\tau\pi)^{-1}$. The width of the low-frequency peak appears to be dominated by exchange broadening, which is supported by the observed field and temperature dependences. From the shift and exchange data it is evident that the xenon of the low-frequency peak is gaslike and in slow exchange with the adsorbed xenon. The existence of pores, indicated by the hysteresis of the isotherm data, may be related to the presence of two distinct sites for xenon.

Ripmeester and Ratcliffe[56] measured the ^{129}Xe NMR spectrum of xenon sorbed in porous vycor glass obtaining two distinct peaks. The authors attribute the high-frequency resonance (~80 ppm) to xenon inside the pores and attribute a resonance near 0 ppm to xenon gas and a "surface phase". Their spectra appear very similar to that of xenon adsorbed on V_2O_5; both spectra have a resonance with a large shift due to strong interactions with the surface and a peak due to gaslike xenon in slow exchange with the strongly adsorbed xenon. Although similar, a direct comparison of the spectra should be approached with caution due to the possible differences in adsorption energy and pore size, both of which directly affect the dynamics that govern the xenon chemical shift.

Conclusions

The chemical shift of ^{129}Xe adsorbed on the surface of TiO_2 (anatase) and on V_2O_5 depends linearly on the xenon coverage, indicating a lack of strong adsorption sites. The contributions to ^{129}Xe chemical shift due to xenon−surface interactions are 109 ± 3 ppm for TiO_2 (anatase) and 93 ± 5 ppm for V_2O_5. V_2O_5/TiO_2 catalysts, particularly those with a high proportion of monomeric vanadyl sites, exhibit strong adsorptive interactions with xenon. The presence of strong adsorption sites on 1.3% and 3.0% V_2O_5/TiO_2 samples excludes the existence of large vanadia domains, indicating that the vanadia units are dispersed on the TiO_2 (anatase) support. Isotherm data show that crystallites of pure V_2O_5 contain a large number of pores. ^{129}Xe NMR of xenon sorbed on V_2O_5 reveals the existence of two distinct environments for xenon. Two-dimensional exchange spectroscopy reveals that xenon diffuses between these two environments; the rates of 0.78, 0.91, and 1.45 ms^{-1} at temperatures of 210, 250, and 290 K show that these environments are within close proximity.

Acknowledgment. This work was supported by the Director, Office of Energy Research, Office of Basic Energy Sciences, Materials Science Division of the U.S. Department of Energy, under Contract DE-AC03-76SF00098. H.C.G. gratefully acknowledges NSF for a fellowship. J.K. thanks DFG for its support. We also acknowledge support from the Shell Development Co. and thank Dr. Eric Munson for a thorough reading of the manuscript.

References and Notes

(1) Gasior, M.; Gasior, I.; Grzybowska, B. *Appl. Catal.* **1984**, *10*, 87.
(2) Wainwright, M. S.; Foster, N. R. *Catal. Rev.* **1979**, *19*, 211.
(3) Bond, G. C.; Konig, P. J. *J. Catal.* **1982**, *77*, 309.
(4) Bosch, H.; Janssen, F. *Catal. Today* **1988**, *19*, 369.
(5) Wachs, I. E.; Saleh, R. Y.; Chan, S. S.; Cherisch, C. C. *Appl. Catal.* **1985**, *15*, 339.
(6) Bond, G. C.; Bruckman, K. *Faraday Discuss. Chem. Soc.* **1981**, *72*, 235.
(7) Eckert, H.; Wachs, I. E. *J. Phys. Chem.* **1989**, *93*, 6796.
(8) Roozeboom, F.; Mittelmeijer-Hazeleger, M. C.; Moulijn, J. A.; Medema, J.; de Beer, V. H.; Gellings, P. J. *J. Phys. Chem.* **1980**, *84*, 2783.
(9) Haber, J.; Kozlowska, A.; Kozlowki, R. J. *J. Catal.* **1986**, *52*, 5831.
(10) Chan, S. S.; Wachs, I. E.; Murrell, L. L.; Wang, L.; Hall, W. K. *J. Phys. Chem.* **1984**, *88*, 5831.

(11) Cristiani, C.; Forzatti, P.; Busca, G. J. *J. Catal.* **1989**, *116*, 586.

(12) Went, G. T.; Leu, L.-J.; Bell, A. T. *J. Catal.* **1992**, *134*, 479.

(13) Ito, T.; Fraissard, J. *J. Phys. Chem.* **1982**, *76*, 5225.

(14) Ito, T.; de Menorval, L. C.; Guerrier, E.; Fraissard, J. *Chem. Phys. Lett.* **1984**, *111*, 271.

(15) Ito, T.; Fraissard, J. *J. Chem. Phys.* **1986**, *83*, 441.

(16) de Menorval, L. C.; Fraissard, J.; Ito, T.; Primet, M. *J. Chem. Soc., Faraday Trans. 1* **1982**, *78*, 403.

(17) de Menorval, L. C.; Fraissard, J.; Ito, T.; Primet, M. *J. Chem. Soc., Faraday Trans. 1*, **1985**, *81*, 2855.

(18) Chen, Q. J.; Fraissard, J. *J. Phys. Chem.* **1992**, *96*, 1809.

(19) Gedeon, A.; Ito, T.; Frassaird, J. *Zeolites* **1988**, *8*, 376.

(20) Tsiao, C.; Corbin, D. R.; Dybowski, C. R. *J. Phys. Chem.* **1991**, *95*, 5586.

(21) Bansal, N.; Dybowski, C. *J. Phys. Chem.* **1988**, *92*, 2333.

(22) Trescos, E.; de Menorval, L. C.; Rachdi, F. *J. Phys. Chem.* **1993**, *97*, 6943.

(23) Boddenberg, B.; Hartmann, M. *Chem. Phys. Lett.* **1993**, *203*, 243.

(24) Ahn, D. H.; Lee, J. S.; Nomura, M.; Sachtler, W. M. H.; Moretti, G.; Woo, S.; Ryoo, R. *J. Catal.* **1992**, *133*, 191.

(25) Moretti, G.; Sachtler, W. M. H. *Catal. Lett.* **1993**, *17*, 285.

(26) Tsiao, C.; Corbin, D. R.; Dybowski, C. R. *J. Phys. Chem.* **1990**, *133*, 191.

(27) Cheung, T. T. P. *J. Phys. Chem.* **1990**, *94*, 376–380.

(28) Ryoo, R.; Pak, C.; Ahn, D. H.; de Menorval, L. C.; Figueras, F. *Catal. Lett.* **1990**, *7*, 417.

(29) Bansal, N.; Dybowski, C. *J. Magn. Reson.* **1990**, *89*, 21.

(30) Ryoo, R.; Liu, S.-B.; de Menorval, L. C.; Takegoshi, K.; Chmelka, B.; Trecoske, M.; Pines, A. *J. Phys. Chem.* **1987**, *91*, 6575.

(31) Chmelka, B. F.; Pearson, J. G.; Liu, S. B.; Ryoo, R.; deMenorval, L. C.; Pines, A. *J. Phys. Chem.* **1991**, *95*, 303–310.

(32) de Menorval, L. C.; Raftery, D.; Lui, S. B.; Takegoshi, K.; Ryoo, R.; Pines, A. *J. Phys. Chem.* **1990**, *94*, 27–31.

(33) Fraissard, J.; Ito, T. *Zeolites* **1988**, *8*, 350–361.

(34) Barrie, P. J.; Klinowski, J. *Prog. NMR Spectrosc.* **1992**, *24*, 91.

(35) Dybowski, C.; Bansal, N.; Duncan, T. M. *Annu. Rev. Phys. Chem.* **1991**, *42*, 433.

(36) Raftery, M. D.; Chmelka, B. F. In *NMR Basic Principles and Progress*; B. Blümich, B., Kosfeld, R., Eds.; Springer-Verlag: Berlin, 1993; Vol. 30, pp 111–158.

(37) Cheung, T. T. P. *J. Phys. Chem.* **1989**, *93*, 7549.

(38) Conner, W. C.; Weist, E. L.; Ito, T.; Fraissard, J. *J. Phys. Chem.* **1989**, *93*, 4138.

(39) Ryoo, R.; Cho, S. J.; Pak, C.; Kim, J.-G.; Ihm, S.-K.; Lee, J. Y. *J. Am. Chem. Soc.* **1992**, *114*, 76.

(40) Ito, T.; Fraissard, J. *J. Chem. Soc., Faraday Trans. 1* **1987**, *83*, 451–462.

(41) Boudart, M.; de Menorval, L. C.; Fraissard, J.; Valenca, G. P. *J. Phys. Chem.* **1988**, *92*, 4033.

(42) Valenca, G. P.; Boudart, M. *J. Catal.* **1991**, *128*, 447.

(43) Boudart, M.; Ryoo, R.; Valenca, G. P.; Van Grieken, R. *Catal. Lett.* **1993**, *17*, 273.

(44) Raftery, D.; Reven, L.; Long, H.; Pines, A.; Tang, P.; Reimer, J. *J. Phys. Chem.* **1993**, *97*, 1649.

(45) Jameson, A. K.; Jameson, C. J.; Gutowsky, H. S. *J. Chem. Phys.* **1970**, *53*, 2310.

(46) Jeener, J.; Meier, B. H.; Bachmann, P.; Ernst, R. R. *J. Chem. Phys.* **1979**, *71*, 4546.

(47) States, D. J.; Haberkorn, R. A.; Ruben, D. J. *J. Magn. Reson.* **1982**, *48*, 286–292.

(48) Topsoe, N.-Y.; Slabiak, T.; Clausen, B. S.; Sruak, T. Z.; Dumesic, J. A. *J. Catal.* **1992**, *134*, 742.

(49) Tanaka, K.; White, J. M. *J. Phys. Chem.* **1982**, *86*, 4708.

(50) Brunauer, S.; Emmet, P. H.; Teller, E. *J. Am. Chem. Soc.* **1938**, *60*, 309.

(51) *Kirk-Othner Concise Encyclopedia of Chemical Technology*; John Wiley & Sons: New York, 1985; p 585.

(52) Gregg, S. J.; S. W., S. K. *Adsorption, Surface Area and Porosity*; Academic Press: New York, 1967; p 177.

(53) Barrett, E. P.; Joyner, L. G.; Halenda, P. P. *J. Am. Chem. Soc.* **1951**, *73*, 373.

(54) Freeman, M. P.; Halsley, G. D. *J. Phys. Chem.* **1956**, *60*, 1119.

(55) Cook, G. A. *Argon, Helium and the Rare Gases*; Interscience: New York, 1961; Vol. 1.

(56) Ripmeester, J. A.; Ratcliffe, C. I. *Anal. Chim. Acta* **1993**, *283*, 1103–1112.

(57) Springuel-Huet, M. A.; Fraissard, J. *Chem. Phys. Lett.* **1989**, *154*, 299–302.

(58) Jameson, C. J.; Jameson, A. K.; Cohen, S. *J. Chem. Phys.* **1973**, *59*, 4540.

(59) Cheung, T. T. P.; Fu, C. M.; Wharry, S. *J. Phys. Chem.* **1988**, *92*, 5170.

(60) Mansfield, M.; Veeman, W. S. *Chem. Phys. Lett.* **1993**, *213*, 153.

(61) *CRC Handbook of Chemistry and Physics*, 66th ed.; CRC Press: Boca Raton, FL, 1985.